JOURNAL OF Materials CHEMISTRY

^{7}Li MAS NMR study of electrochemically deintercalated $Li_xNi_{0.30}Co_{0.70}O_2$ phases: evidence of electronic and ionic mobility, and redox processes

Dany Carlier, Michel Ménétrier and Claude Delmas*

Institut de Chimie de la Matière Condensée de Bordeaux-CNRS and Ecole Nationale Supérieure de Chimie et Physique de Bordeaux, Av. Dr A. Schweitzer, 33608 Pessac cedex, France. E-mail: delmas@icmcb.u-bordeaux.fr

Received 31st July 2000, Accepted 2nd October 2000
First published as an Advance Article on the web 4th December 2000

$Li_xNi_{0.30}Co_{0.70}O_2$ phases obtained by electrochemical deintercalation have been characterised by XRD, ^{7}Li MAS NMR, electronic conductivity and thermoelectronic power measurements. Ni^{3+} oxidation to Ni^{4+} occurs at the onset of deintercalation, leading to Ni^{3+}/Ni^{4+} hopping which causes an exchange of the ^{7}Li NMR signals, characteristic of a contact shift due to paramagnetic low spin Ni^{3+}. Depending on composition and temperature, the presence or absence of lithium ions, which only interact with diamagnetic Co^{3+} ions, allows discrimination between an electronic and an ionic exchange phenomenon. For x close to 0.70, Ni/Co hopping ($Ni^{4+} + Co^{3+} \leftrightarrow Ni^{3+} + Co^{4+}$) is evidenced, which makes the question as to which ion is actually oxidised during deintercalation somewhat irrelevant. Finally, for $x < 0.70$, the presence of Ni ions hinders true long range electronic delocalisation, but low spin Co^{4+} ions are clearly not localised, as evidenced by the NMR data and the thermoelectronic power coefficient.

Introduction

The Li_xNiO_2 and Li_xCoO_2 systems are particularly interesting as positive electrode materials for lithium ion batteries because they lead to a high cell voltage and good cycling properties. $LiCoO_2$ has been used since 1994 in commercial lithium batteries, but the high cost of cobalt has induced an extensive search for other materials. The Li_xNiO_2 system could be a good candidate, but the instability of Li_xNiO_2 for low x values leads to safety problems which require cationic substitution for nickel to optimise the material's properties. Among them, cobalt substitution for nickel plays an important role. The $Li_xNi_yCo_{1-y}O_2$ systems have been extensively studied in the past few years.[1–9] These materials exhibit a strictly layered α-$NaFeO_2$-type structure when $y \geqslant 0.3$: for smaller cobalt ratios, some Ni^{2+} ions remain in the interslab space.[1,10] This layered structure is built from alternate sheets of $(Ni,Co)O_6$ and of LiO_6 octahedra sharing edges. In this structure, nickel and cobalt ions are in the trivalent low spin state.[5] The Co^{3+} ions are diamagnetic ($t_{2g}^6 e_g^0$), whereas the Ni^{3+} ions are paramagnetic ($t_{2g}^6 e_g^1$), which could lead to a Jahn–Teller distortion. Rougier *et al.* discovered, using X-ray absorption analysis, the presence of a local Jahn–Teller distortion of the NiO_6 octahedra in $LiNiO_2$.[11] Nakaï and Nakagome also showed that the local Jahn–Teller distortion is reduced by cobalt doping.[12]

It appears that knowledge of the local structure in positive electrode materials is crucial for the understanding of their electrochemical properties. Therefore, as a complement to X-ray diffraction studies, which yield long range structural information, we used ^{7}Li NMR, which is a good probe for the characterisation of the local lithium environment in these systems, making use of the hyperfine interactions due to their paramagnetic or metallic character. Indeed, ^{6}Li/^{7}Li NMR spectroscopy has been used many times to study lithium transition metal oxide positive electrode materials, starting with $LiNi_yCo_{1-y}O_2$ and $LiMn_2O_4$ in 1994.[13,14] In 1995, Marichal *et al.* used ^{6,7}Li MAS NMR to characterise the Li^+ ions with paramagnetic Ni^{3+} ions as first and second neighbours in the former systems.[15] $LiMn_2O_4$ and other lithium manganates were also widely investigated,[16–19] as well as $LiCoO_2$ (stoichiometric or non-stoichiometric).[20–27]

However, ^{6}Li/^{7}Li NMR spectroscopy has not been extensively applied to the study of electrochemically deintercalated materials. Saadoune *et al.* used ^{7}Li static NMR experiments to study the deintercalation process in the $LiNi_{0.10}Co_{0.90}O_2$ and $LiNi_{0.20}Co_{0.80}O_2$ systems.[28] This study confirmed that the Ni^{3+} ions were oxidised first and that oxidation of Co^{3+} ions occurred in the final process. Nevertheless, static experiments offer poor resolution in these systems, compared to magic angle spinning NMR. Indeed, ^{7}Li MAS NMR was recently used to study Li_xCoO_2 deintercalated phases.[24–27] In particular, these studies highlighted a semiconductor to metal transition upon deintercalation through the appearance of a Knight-shift signal for the metallic phases.[26] Very recently, Lee *et al.* used ^{6}Li/^{7}Li MAS NMR to study the changes in local structure after charging $LiMn_2O_4$ to different lithium amounts.[29]

In all these studies, the question of electronic mobility was mentioned by Lee *et al.* in $LiMn_2O_4$, who considered that the "normal" Li ions interact with an average "$Mn^{3.5+}$" ion, due to rapid electronic hopping between Mn^{3+} and Mn^{4+}. In Li_xCoO_2, Ménétrier *et al* considered that the small number of localised Co^{4+} ions present for $0.94 \leqslant x \leqslant 1$ interact with a large number of Li^+ ions (making them not observable by NMR), due to the Co^{4+}/Co^{3+} hopping.[26] However, for smaller x values, electronic delocalisation leads to a Knight shift which involves all Li ions in the material. In order to characterise the effect of electronic hopping upon deintercalation, we selected the $Li_xNi_{0.30}Co_{0.70}O_2$ system, where the localised Ni^{3+} ions lead to a well-resolved fine structure in the starting material: each Ni^{3+} ion influences (differently) its 1st and 2nd neighbour Li^+ ions.

We therefore performed a detailed study of the $Li_xNi_{0.30}Co_{0.70}O_2$ system for $0.40 \leqslant x \leqslant 1$ by X-ray diffraction, ^{7}Li MAS NMR and electrical measurements in order to follow the oxidation of paramagnetic Ni^{3+} ions into diamagnetic Ni^{4+}

 DOI: 10.1039/b006179o

and of diamagnetic Co^{3+} ions into Co^{4+} upon lithium deintercalation, and to ascertain the effect of electronic and ionic mobility on the NMR spectra. In a preliminary section, we first discuss further the assignment of NMR signals observed for the non-deintercalated material.

Experimental

Synthesis

The $LiNi_{0.30}Co_{0.70}O_2$ starting material was prepared by direct reaction from Li_2CO_3, NiO and Co_3O_4 in stoichiometric proportions. The mixture was heated under O_2 at 600 °C for 10 h, 800 °C for 48 h and three times at 900 °C for 20 h with intermediate grinding. Chemical analysis conducted by inductively coupled plasma (ICP) absorption spectroscopy, yielded Ni/(Ni+Co), Co/(Ni+Co) and Li/(Ni+Co) molar ratios which lead to the $Li_{0.99}Ni_{0.30}Co_{0.70}O_2$ formula.

Electrochemical characterisation

Electrochemical studies were carried out with Li/liquid electrolyte/$LiNi_{0.30}Co_{0.70}O_2$ cells. $LiClO_4$ in propylene carbonate was used as the electrolyte for $0.60 \leqslant x < 1$ and $LiPF_6$ in ethylene carbonate–dimethyl carbonate–propylene carbonate for $0.40 \leqslant x < 0.60$ (Merck, ZV1011 Selectipur). For classical electrochemical experiments, the positive electrode consisted of a mixture of 88% by weight of active material, 2% PTFE [poly(tetrafluorethylene)] and 10% carbon black. For electrochemical preparation of deintercalated phases for X-ray diffraction, ^{7}Li MAS NMR and electrical measurements, sintered pellets (8 mm of diameter, 780 MPa compression followed by a thermal treatment of 12 h at 900 °C under oxygen) of the starting material were used as positive electrodes without additive. The cells assembled in an argon-filled dry box were charged at very low current density (C/600 *i.e.* 600 h are needed to remove one Li from the formula). Before recovering the positive electrode, the cells were allowed to relax until their open-circuit voltage varied by no more than 1 mV h^{-1}.

X-Ray diffraction study

The X-ray diffraction patterns of the non-deintercalated compound were recorded using a Siemens D5000 powder diffractometer with Cu-Kα radiation and a graphite diffracted beam monochromator, whereas diffraction data for the $Li_xNi_{0.30}Co_{0.70}O_2$ phases were collected on an INEL CPS 120 curve position sensitive detector using Co-Kα radiation and sealed capillaries (under dry argon).

NMR experiments

^{7}Li MAS NMR spectra were recorded on a Bruker MSL200 spectrometer at 77.7 MHz, with a standard 4 mm Bruker MAS probe. The samples were mixed with dry silica (typically 50% in weight), in order to facilitate spinning and improve the field homogeneity, since they may exhibit metallic or paramagnetic properties. The mixture was placed into a 4 mm diameter zirconia rotor in the dry box. Spinning speeds (ν_r) of 10 and 15 kHz were used. For all phases, two types of sequence were systematically used: a single pulse sequence and a Hahn echo sequence (rotor-synchronised pulses). The single pulse sequence with $t_{\pi/2} = 3.05$ μs requires a first-order phasing process and a $\sin x/x$ baseline correction due to the dead time of the spectrometer. The Hahn echo sequence [$t_{\pi/2}$–τ_1–t_π–τ_2] was utilised in order to facilitate the phasing of all the signals and of their spinning sidebands and to ensure the observation of possibly very wide signals which are lost during the receiver dead time. The 90° pulse duration used ($t_{\pi/2}$) was also equal to 3.05 μs. In order to synchronise the spin echo with the first rotational echo, τ_1 was fixed to the rotor period $T_r = 1/\nu_r$. With such a Hahn echo sequence, phasing can be done easily with only zero-order correction, if required, and no baseline correction is needed. The shape of spectra recorded with the Hahn echo sequence helped us to execute the sometimes delicate phasing and baseline correction of those recorded with the single pulse sequence. A 200 kHz spectral width was used, and the recycle time, $D_0 = 1$ s, is long enough to avoid T_1 saturation effects. The isotropic shifts, reported in parts per million, are relative to an external sample of 1 M LiCl solution in water.

The inversion-recovery measurements were recorded with an appropriate sequence [t_π–τ_1–$t_{\pi/2}$] were τ_1 is variable. One can thus follow, as a function of τ_1, the quantity of signal which is longitudinally relaxed. If $\tau_1 = \ln 2 * T_1$, for one signal with longitudinal relaxation time T_1, all the magnetisation is placed in the detector plan after the τ_1 delay, so that no signal is recorded after the recovery pulse. From this τ_1 value, we extracted an approximate T_1 value for the signal concerned.

Electronic conductivity and thermoelectronic measurements

For electronic conductivity measurements, a four-probe method was used with direct current in the 100–300 K range. The thermoelectronic measurements were carried out by using equipment described elsewhere.[30]

NMR theoretical background (contact shifts)

The hyperfine coupling between a nucleus and unpaired electrons gives rise to a shift and a broadening of the NMR signals. The hamiltonian of the hyperfine interaction, H_{SI}, between unpaired electrons with $\hat{S}$ total electron spin operator and a nucleus with $\hat{I}$ spin operator can be separated into two terms:

$$H_{SI} = A_c \hat{I}\hat{S} + \hat{I}\tilde{A}_{dip}\hat{S} \quad (1)$$

where A_c is the Fermi contact coupling constant and $\tilde{A}_{dip}$ the dipolar tensor for the electron–nucleus coupling. The Fermi contact is due to the presence of a certain density of paramagnetic electrons in a spherical orbital and, therefore, at the site of the nucleus. This interaction gives rise to large shifts and is usually called "contact shift" or "Fermi contact".

The shift induced by the Fermi contact in materials with 3d metal ions can be expressed as:[31,32]

$$\frac{\Delta\omega}{\omega_0} = -\frac{A_c}{\omega_0 \hbar}\langle S_z \rangle \quad (2)$$

where the sign of the Fermi constant, A_c, will give the direction of the shift. A_c is dependent on the paramagnetic spin density at the nucleus $\rho(r=0)$ (eqn. 3):

$$\left(\frac{A_c}{h}\right) = \frac{\mu_0}{3S} g \mu_B \gamma_N \rho(r=0) \quad (3)$$

where

$$\rho(r=0) = \sum_i [|\Psi_i\uparrow(0)|^2 - |\Psi_i\downarrow(0)|^2].$$

$|\Psi_i\uparrow(0)|^2$ is the probability of having a spin positively polarised (*i.e.* with the same polarisation as the applied magnetic field) at the nucleus and $|\Psi_i\downarrow(0)|^2$ is the probability of having a spin negatively polarised at the nucleus. (A_c/h) is expressed in (rad s^{-1}) and $\rho(r=0)$ is in m^{-3}. The time averaged value of the electron spin, $\langle S_z \rangle$ in eqn. 2, is proportional to the magnetic molar susceptibility, χ (m^3 mol^{-1}) and can be expressed as:[33]

$$\langle S_z \rangle = -g\mu_B \omega_0 \frac{S(S+1)}{3\gamma_N kT} \quad (4)$$

Only the average value of S_z is meaningful with respect to the

NMR experiment since electrons relax several orders of magnitude faster than the coupling frequency A_c/h (Hz).

The Fermi contact is considered to be additive, so that the shift due to many magnetic ions may be considered as the sum of the shifts induced by each magnetic ion on the nucleus studied. Sometimes, the shift is so large that signals are situated in a completely different range than for a similar diamagnetic compound, or even not observable.[33]

The other contribution to the hyperfine coupling is the dipolar interaction which occurs through space. In contrast to the Fermi contact term, this interaction contains an anisotropic contribution and is averaged out to an isotropic component if the NMR spectrum is recorded under fast enough magic angle spinning. The isotropic contribution thus obtained is known as "dipolar shift" or pseudocontact shift. As we are limited by the rotation speed of the sample, some of the anisotropic part of the dipolar shift remains in the line width. The extent of the width depends on the proximity of the unpaired electron and the nucleus.

The observed isotropic shift is the sum of the Fermi contact and the pseudocontact shifts. Since the isotropic contribution to the pseudocontact interaction is zero for an isotropic $\tilde{g}$ tensor, the pseudocontact shift is generally smaller than the Fermi contact shift. The Fermi contact term was thus considered to be predominant in the shift magnitude for several oxides,[16,18,34] and this should also be true for the $Li_xNi_yCo_{1-y}O_2$ systems.

The magnitude of the contact shift in this system depends on the overlap between the 2s orbital of the Li^+ ion and the t_{2g} and e_g orbitals of the 3d ions. The overlap can occur directly or *via* the oxygen orbitals. Goodenough and Kanamori established rules which are usually applied to determine the type of the magnetic coupling (ferromagnetic or antiferromagnetic) between magnetic ions,[35] but we can transpose them to determine the sign and the magnitude of the contact shift. The spectrometer magnetic field gives the orientation of the 3d paramagnetic electrons. We then apply the Goodenough–Kanamori superexchange mechanisms to predict the sign of the spin density transferred onto the Li 2s orbital. These rules consider three principal contributions: a correlation effect, a delocalisation effect, and a polarisation effect. As the polarisation effect is small compared to the other two,[35] only the correlation and delocalisation superexchange mechanisms are considered in our prediction. A positive spin density predicted in the 2s orbital will lead to an additive local field which yields a positive shift (see eqn. 2 and 3). On the other hand, a negative spin density predicted in the s orbital will lead to a negative shift. We will use these transposed Goodenough–Kanamori rules to assign the signals of the $LiNi_{0.30}Co_{0.70}O_2$ spectrum.

Results and discussion

NMR spectra of the non-deintercalated phase $LiNi_{0.30}Co_{0.70}O_2$

Marichal *et al.* recorded ^6Li and ^7Li static and MAS NMR spectra for the $LiNi_{1-y}Co_yO_2$ solid solution.[15] It appears that ^6Li MAS NMR offers a higher resolution while better sensitivity is obtained in ^7Li resonances. Nevertheless, the spectra present the same general features. We decided to use ^7Li MAS NMR to obtain better sensitivity and a 15 kHz spinning speed to get reasonably good resolution: the signals and spinning side bands do not overlap.

Fig. 1 shows the ^7Li NMR spectrum of the non-deintercalated $LiNi_{0.30}Co_{0.70}O_2$ phase. Several signals are recorded: a signal at 0 ppm, a broad peak centred at 110 ppm and others situated at −15, −30 and −45 ppm. Close inspection of the broad signals shows a series of equidistant peaks *ca.* 15 ppm apart from each other. For a better understanding of the signal assignments, Marichal *et al.* used two variables, p_1 and p_2,

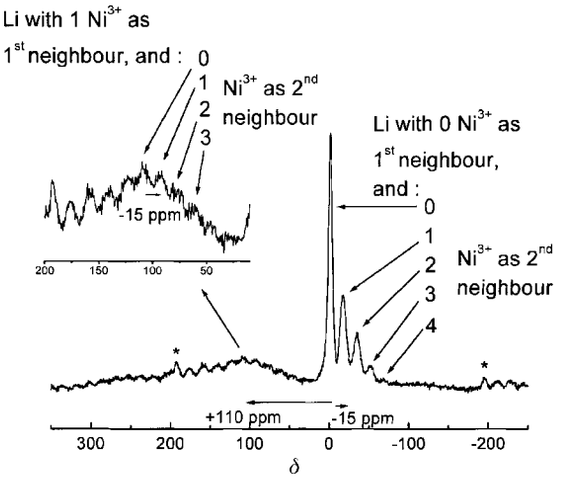

Fig. 1 ^7Li MAS NMR spectrum of $LiNi_{0.30}Co_{0.70}O_2$ recorded with the single pulse sequence with a 15 kHz spinning speed (* denotes spinning sidebands).

which indicate, respectively, the number of 1st and 2nd cationic Ni^{3+} neighbours of a given Li^+ ion.[15] In Fig. 1, the peak situated at 0 ppm is assigned to Li^+ ions interacting only with diamagnetic Co^{3+} ions as 1st and 2nd neighbours ($p_1=0$, $p_2=0$). We also find this lithium environment in stoichiometric $LiCoO_2$, where all cobalt ions are diamagnetic: the MAS NMR spectrum presents a single signal situated at 0 ppm.

The signals situated at −15, −30 and −45 ppm are assigned to Li^+ ions interacting with only Co^{3+} ions as 1st neighbours ($p_1=0$) and with, respectively, one ($p_2=1$), two ($p_2=2$) and three ($p_2=3$) Ni^{3+} ions as 2nd neighbours. In the same way, signals situated at +110, +95, +80 and +65 ppm are assigned to Li^+ ions interacting with one Ni^{3+} ion as 1st neighbour ($p_1=1$) and respectively zero ($p_2=0$), one ($p_2=1$), two ($p_2=2$), three ($p_2=3$) Ni^{3+} ions as 2nd neighbours. A very broad signal around 100–400 ppm is also observed and is probably due to lithium ions interacting with more than one Ni^{3+} as 1st neighbours ($p_1>1$).

At that time, the assignment was not fully explained and was principally based on the fact that the Li–Ni interaction presents a larger dipolar component for shorter Li–Ni distances. Therefore, the signals at +110 ppm which were broader than those at −15, −30 and −45 ppm are assigned to lithium interacting with Ni^{3+} as 1st neighbour. We try here to give other reasons for this assignment.

The Li^+–Ni^{3+} 1st neighbour interaction occurs at 90° *via* oxygen orbitals (Fig. 2a) and is written as e_g–p_σ–p_σ'–s. The transposed Goodenough–Kanamori superexchange rules are applied to determine the magnitude and the sign of the transferred electronic density on the lithium nucleus. Whatever mechanism is considered (double correlation or delocalisation), this 90° Ni–O–Li interaction yields a positive shift (*i.e.* a spin polarisation identical to that due to the applied magnetic field). The Li^+–Ni^{3+} 2nd neighbour interaction occurs at 180° *via* one oxygen orbital (Fig. 2b) and is written as e_g–p_σ–s. In this case, the superexchange mechanism by delocalisation yields a positive shift, whereas that by correlation yields a negative one. In this respect, the attribution of the observed positive and negative paramagnetic shifts to the 90 and 180° Ni–O–Li indirect couplings, respectively, agrees with the transposed superexchange rules. Indeed, the correlation mechanism with 180° geometry is the only one that leads to a negative shift. The amplitude can be also evaluated, because, in the case of the 180° interaction, the two mechanisms lead to opposite signs. The resulting shift may therefore be smaller than the shift predicted for the 90° interaction, for which both mechanisms give the same sign. Furthermore, two different pathways

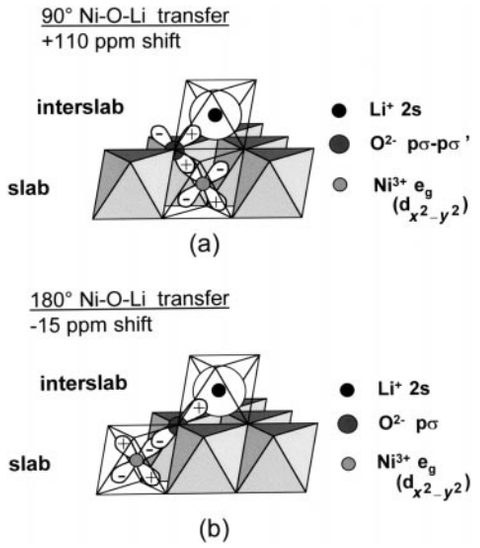

Fig. 2 The two types of paramagnetic Li^+–Ni^{3+} interaction leading to a contact shift: (a) the 90° transfer and (b) the 180° transfer. This figure symbolises the overlap of the (same sign) orbital lobes. The sign of the transferred electron spin density is discussed in the text.

(involving two different oxygen ions) can operate for a given Ni–Li pair with the 90° geometry, and only one pathway for the 180° geometry. Note also that the Ni–O–Li angles found by Rietveld refinement in $LiNi_{0.30}Co_{0.70}O_2$ are 90.4 and 173.7°. The 90.4° Ni–O–Li angle is thus not much different from 90° so that the transposed Goodenough–Kanamori rules should apply fully, but the 173.7° Ni–O–Li angle is somewhat more different from the ideal angle considered for the superexchange rules. The magnitude of the transferred spin density may therefore be weaker than that predicted, because the e_g–p_σ–s overlap is weaker, even though the overlap with an s orbital is less sensitive to angles than in the case of a d orbital.

The sign of the shift given for the 90 and 180° interactions supposes that Ni^{3+} ions are not strongly Jahn–Teller distorted. Indeed, in such a case, a positive shift would be expected for the 180° interaction, whereas the 90° interaction could yield a positive or negative shift, depending on the mechanism considered (superexchange by delocalisation yields a negative shift, whereas superexchange by double correlation yields a positive shift). However, the width of the signals confirms the assignment given above, because they are broader for lithium ions interacting with Ni^{3+} as 1st neighbour, as the dipolar interaction depending on the electron–nucleus distance is stronger. The Jahn–Teller distortion, which is in any case non-cooperative,[11] must therefore be weak for our material. This is consistent with the fact that the amount of cobalt is high, and must therefore reduce the Jahn–Teller distortion of the NiO_6 octahedra as shown by Nakaï *et al.*[12] However, the only way to ascertain the assignment and to predict shifts in other cases, in particular if the angles differ from 90° and 180° (as in $LiMn_2O_4$ spinel phases), would be theoretical calculations of the polarised spin density at the nucleus. Such calculations are not currently used in the NMR field. Recently, Maruta *et al.* performed DFT calculations to evaluate the electron spin density distribution at the hydrogen atoms of the 4-hydroxyamino TEMPO compound.[36] Heise *et al.* also performed calculations of the spin distribution in nitronylnitroxides;[37] but to our knowledge, no *ab initio* calculation of the Fermi contact shift has been performed in non-molecular solids.

Taking eqn. 2, 3 and 4 using $S=1/2$ and $g=2.137$ (a value given by Stoyanova *et al.*[38]) the density of spin at the nucleus responsible for the observed shift can be calculated. The signal at +110 ppm assigned to Li^+ interacting with Ni^{3+} as 1st neighbour is thus due to a spin density of $+0.00544\ Å^{-3}$ and the signal at −15 ppm assigned to Li^+ interacting with Ni^{3+} as 2nd neighbour to a spin density of $-0.00074\ Å^{-3}$.

Deintercalated $Li_xNi_{0.30}Co_{0.70}O_2$ phases

The $Li_xNi_{0.30}Co_{0.70}O_2$ deintercalated phases were obtained from the $LiNi_{0.30}Co_{0.70}O_2$ starting material, whose XRD pattern is characteristic of a layered α-$NaFeO_2$-type structure. The hexagonal cell parameters are $a_{hex}=2.83408(6)$ and $c_{hex}=14.1009(1)$ Å. The Rietveld refinement ($R_{wp}=18.6$, and $R_B=4.89\%$) shows that the cobalt ions occupy the 3a position of the $R\bar{3}m$ space group, the lithium ions the 3b position and the oxygen ions the 6c position with $z=0.2596(6)$. This refinement confirms that no nickel ions are present in the lithium sites.

Electrochemical study

Fig. 3 shows the first galvanostatic charge and discharge curves of an $Li//Li_xNi_{0.30}Co_{0.70}O_2$ cell at low rate (*C*/100, 100 h to extract one lithium). It shows a smooth potential jump around $x=0.70$ which separates two continuous domains. This curve does not exhibit any voltage plateau associated with the existence of a two-phase domain as it occurs in $LiCoO_2$[39] and $LiNiO_2$.[40] At the beginning of the charge, the electrochemical curve is similar to that of an $Li//Li_xNiO_2$ cell, whereas, for $x<0.7$, the curve is similar to that of an $Li//Li_xCoO_2$ cell. This fact, coupled with static NMR experiments on the $Li_xNi_{0.10}Co_{0.90}O_2$ and $Li_xNi_{0.20}Co_{0.80}O_2$ phases and magnetic measurements, suggested to Saadoune *et al.* that, in these phases, Ni^{3+} ions are oxidised first, whereas oxidation of the Co^{3+} ions occurs in the second part of the process.[28]

X-Ray diffraction study

Each deintercalated $Li_xNi_{0.30}Co_{0.70}O_2$ phase chosen for the NMR experiments was also studied by XRD. All the materials exhibit narrow peaks, indicating the persistence of the good crystallinity throughout the electrochemical deintercalation. All the XRD patterns are characteristic of monophasic materials and can be indexed in the trigonal $R\bar{3}m$ space group. Fig. 4 shows the evolution of the hexagonal cell parameters during deintercalation. The c_{hex} parameter, which is linked to the interslab distance, increases as the amount of lithium extracted increases. This evolution is explained by the strengthening of the repulsive interaction between the oxygen atoms of adjacent layers after deintercalation. The decrease of the a_{hex} parameter (metal–metal intrasheet distance) upon deintercalation is caused by the appearance of Ni^{4+} and/or Co^{4+} which have smaller radii than Ni^{3+} and Co^{3+}. These evolutions are similar to those of most A_xMO_2 lamellar oxides.[1,41]

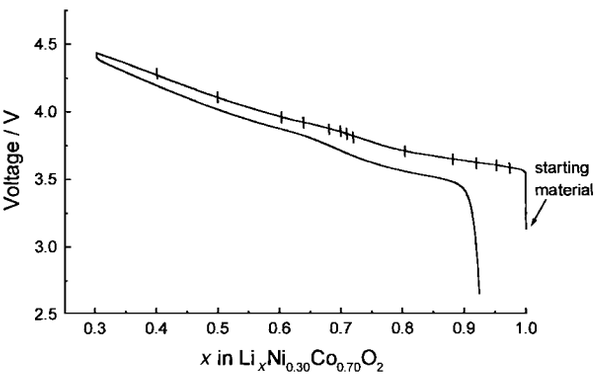

Fig. 3 First galvanostatic charge and discharge of an $Li//Li_xNi_{0.30}Co_{0.70}O_2$ electrochemical cell (*C*/100 rate). Compositions studied by NMR and electrical measurements are indicated.

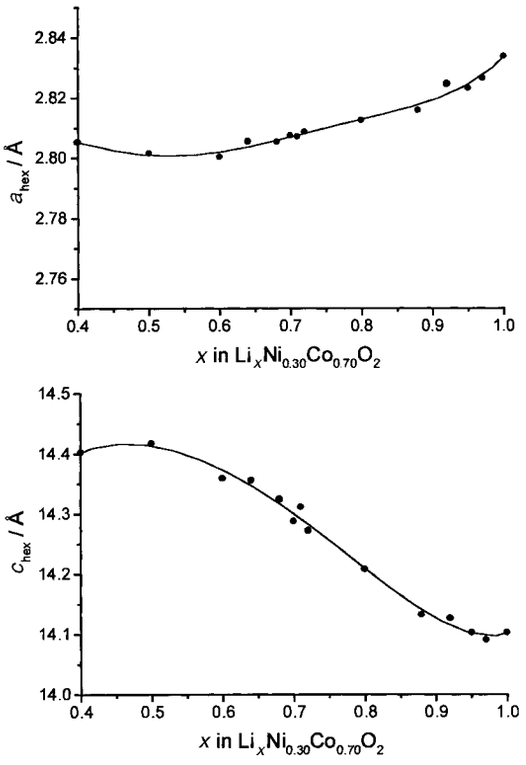

Fig. 4 Variation of the hexagonal cell parameters for $Li_xNi_{0.30}Co_{0.70}O_2$ phases ($0.40 \leqslant x \leqslant 1$).

^{7}Li MAS NMR study

Fig. 5 shows the MAS NMR spectra recorded for the $Li_xNi_{0.30}Co_{0.70}O_2$ ($0.40 \leqslant x \leqslant 1$) phases with a 15 kHz spinning speed and a single pulse sequence. As x decreases, the signals assigned to lithium ions interacting with Ni^{3+} ions as 1st or 2nd neighbour disappear progressively, while a new signal appears. This signal, which becomes apparent for $x \leqslant 0.80$, is situated at 57 ppm for $x = 0.80$; its shift decreases for $x > 0.70$ and increases for $x < 0.70$ upon deintercalation.

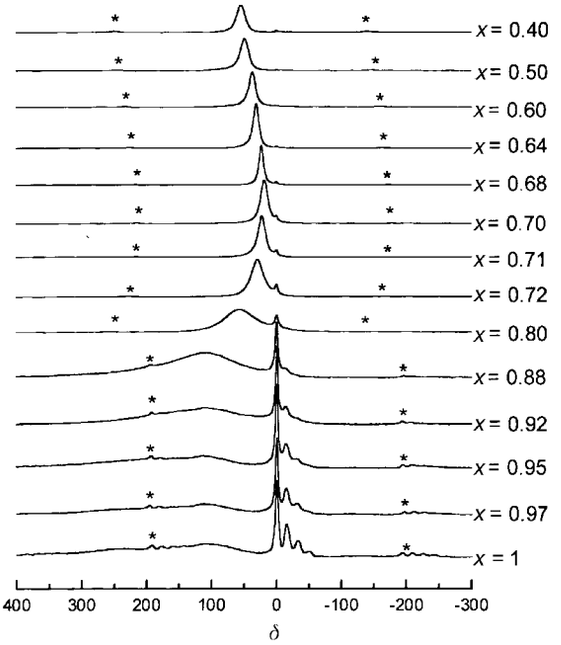

Fig. 5 ^{7}Li MAS NMR spectra ($\nu_r = 15$ kHz) for the various $Li_xNi_{0.30}Co_{0.70}O_2$ phases ($0.40 \leqslant x \leqslant 1$), recorded with the single pulse sequence, plotted against an arbitrary intensity scale (* denotes spinning side bands).

For more clarity, the discussion on these data will be divided into two parts.

Initial deintercalation. First, the evolution of the ^{7}Li MAS NMR spectra confirms that lithium deintercalation induces nickel oxidation, since the signals due to lithium ions interacting with paramagnetic Ni^{3+} ions as 1st or 2nd neighbour disappear: paramagnetic Ni^{3+} ions are oxidised into diamagnetic Ni^{4+} ions, which induce no contact shift. Nevertheless, the disappearance of the fine structure cannot be only due to Ni^{3+} oxidation leading to localised Ni^{4+}, because, for $x = 0.80$ no signal assigned with Ni^{3+} as 1st or 2nd neighbour is observed, whereas at least 0.10 Ni^{3+} remain for this composition. Indeed, we know that even 10% of Ni^{3+} ions yield the "1st and 2nd neighbour" fine structure.[15]

Analysis of the spectra obtained by spin echo and single pulse sequences provides information on the origin of the new signal. Fig. 6 shows the ^{7}Li MAS NMR spectra of the $LiNi_{0.30}Co_{0.70}O_2$ and $Li_{0.80}Ni_{0.30}Co_{0.70}O_2$ phases recorded with the single pulse sequence and the Hahn echo (rotor-synchronised echo) sequence. In Fig. 6a the broad signals at 100–400 ppm, due to lithium interacting with more than one Ni^{3+} ion, are more visible at high shift values with the rotor-synchronised sequence. Indeed, parts of broad signals are lost in the receiver dead time, unavoidable with a single pulse sequence. A rotor-synchronised echo sequence leads to a refocusing of the magnetisation and is better adapted for the observation of such wide signals. We might expect, therefore, that the new broad signal emerging in the deintercalated phases will be seen more clearly with the rotor-synchronised echo sequence. In fact, it is obvious that the single pulse sequence gives a better observation of this signal (Fig. 6b). This can be explained by the existence of mobility in the materials which, for the rotor-synchronised echo sequence, leads to the signals concerned with this mobility not being refocused. Indeed, mobility induces a change in the spin system between the two pulses of the echo, so that the 180° pulse cannot refocus the magnetisation.[42] Comparison of the spectra shows that the new signal is caused by mobility in the system, leading to an NMR exchange phenomenon. We show here spectra recorded with the two types of sequences for $Li_{0.80}Ni_{0.30}Co_{0.70}O_2$ only, but

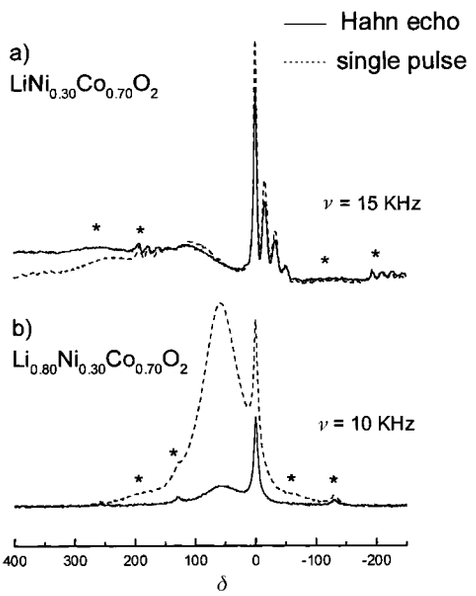

Fig. 6 ^{7}Li MAS NMR spectra of the $LiNi_{0.30}Co_{0.70}O_2$ and $Li_{0.80}Ni_{0.30}Co_{0.70}O_2$ phases recorded with the single pulse and the Hahn echo sequences. Spectra are plotted against an absolute intensity scale, taking into account the sample mass and the number of acquisitions. The spinning speed is indicated for each composition (* denotes spinning side bands).

this fact holds for all the phases that are deintercalated enough to present the new signal.

We also performed inversion-recovery measurements on several deintercalated phases. These experiments allow us to approximate the T_1 value for each signal. They clearly show for $LiNi_{0.30}Co_{0.70}O_2$ that the two groups of signals assigned to lithium ions interacting with "Ni^{3+} 1st and 2nd neighbours" invert at the same time ($T_1 = 4$ ms), whereas the signal at 0 ppm assigned to lithium ions interacting only with cobalt inverts later ($T_1 = 8$ ms). Indeed, ions interacting with paramagnetic neighbours have shorter T_1 time than those interacting with diamagnetic ions. The inversion-recovery measurements on deintercalated phases show that the new broad signal has the same T_1 as the signals assigned to lithium ions interacting with "Ni^{3+} 1st and 2nd neighbours" ($T_1 = 3$ ms for $x = 0.88$), whereas the 0 ppm signal still has a longer T_1 ($T_1 = 6$ ms for $x = 0.88$). These measurements show that the disappearance of the "Ni^{3+} 1st and 2nd neighbours" signals is linked with the emergence of the new signal. Nevertheless, 2D exchange NMR measurements would ascertain which signals are involved in the exchange phenomenon.

Variable temperature NMR spectra for $Li_{0.95}Ni_{0.30}Co_{0.70}O_2$. Since mobility is involved in the emergence of the new signal, we selected a compound with weak mobility and we tried to increase it by heating. Fig. 7 shows the ^{7}Li MAS NMR spectra recorded with the single pulse sequence as a function of temperature for the $Li_{0.95}Ni_{0.30}Co_{0.70}O_2$ phase. Few Ni^{3+} ions are oxidised in this phase, so that the "Ni^{3+} 1st and 2nd neighbours" fine structure remains observable at room temperature. As temperature is increased from 295 to 403 K, several observations can be made.

(1) The "Ni^{3+} 1st and 2nd neighbours" paramagnetic signals are less and less shifted. This evolution toward 0 ppm as temperature increases is typically observed for paramagnetic shifts. Indeed, as temperature increases, the time-averaged amount of polarised electrons decreases as the magnetic susceptibility decreases. The magnitude of the contact shift therefore decreases under a temperature increase as given by eqn. 2 and 4.

(2) The "Ni^{3+} 1st and 2nd neighbours" signals progressively disappear and a new large signal appears. This behaviour confirms that mobility exists in the deintercalated phases and leads to an averaged NMR signal due to an exchange phenomenon, which is activated by heating.

(3) The position of the averaged signal could appear surprising, because it is more shifted than the signal assigned to Li^+ ions interacting with one Ni^{3+} as 1st neighbour. Indeed, we first expected to record this averaged signal between those of Li^+ ions interacting with one Ni^{3+} ion as 1st neighbour and those of Li^+ ions interacting with Ni^{3+} ions as 2nd neighbours. However, one must consider the other lithium environments with more than one Ni^{3+} as 1st neighbour, which are also involved in the exchange phenomenon. These signals are more shifted than that for one "Ni^{3+} as 1st neighbour", but are not clearly observed in our spectra, because of their excessive widths and, consequently, overlapping character.

(4) The intensity of the signal, situated at 0 ppm, of lithium ions with only Co^{3+} neighbours does not decrease. If the exchange phenomenon observed was due to ionic mobility, every lithium ion would be involved in the exchange phenomenon, even those with only diamagnetic Co^{3+} as 1st and 2nd neighbours, but the intensity of this signal remains approximately the same as the temperature increases. The exchange phenomenon is therefore due to electronic mobility around the Li^+ ion. Indeed, as lithium is deintercalated, paramagnetic Ni^{3+} ions are oxidised and lead to diamagnetic Ni^{4+} ions. Ni^{3+}/Ni^{4+} electronic hopping may then occur. Lithium ions with nickel ions as 1st and 2nd neighbours now interact with nickel ions rapidly oscillating between the 3+ and 4+ oxidation states on the NMR time scale ($\approx 10^{-6}$ s). This electronic hopping gets quicker upon heating, as can be seen in Fig. 7.

In Fig. 5, it can be observed that the averaged signal discussed above is less and less shifted as the lithium amount decreases to $x = 0.70$. Indeed, as the number of diamagnetic Ni^{4+} ions involved in the Ni^{3+}/Ni^{4+} electronic hopping phenomenon increases, the average density of unpaired electron spin seen by the lithium ions concerned decreases.

Variable temperature NMR spectra for $Li_{0.80}Ni_{0.30}Co_{0.70}O_2$. We noted that lithium deintercalation involves Ni^{3+} oxidation, but it also involves Li^+ vacancies. In order to increase the ionic mobility, we recorded the NMR spectra of the $Li_{0.80}Ni_{0.30}Co_{0.70}O_2$ phase at different temperatures (Fig. 8); this phase presents a higher mobility than $Li_{0.95}Ni_{0.30}Co_{0.70}O_2$. At room temperature, the former compound shows an averaged signal, no trace of the "Ni^{3+} 1st and 2nd neighbours" fine structure and the signal at 0 ppm assigned to lithium ions interacting only with Co^{3+} as 1st and 2nd neighbours. The Ni^{3+}/Ni^{4+} electronic hopping phenomenon can thus be considered as rapid, whereas the ionic mobility is not seen by NMR, as it is for the $x = 0.95$ compound at 400 K. As the temperature increases, the averaged signal shifts

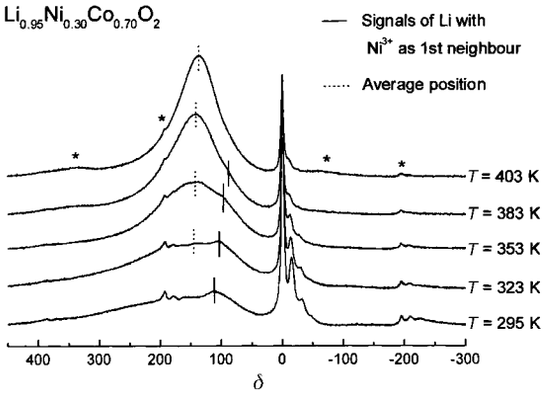

Fig. 7 ^{7}Li MAS NMR spectra of $Li_{0.95}Ni_{0.30}Co_{0.70}O_2$ recorded with the single pulse sequence at various temperatures. Spectra are plotted against an absolute intensity scale, taking into account the number of acquisitions (* denotes spinning side bands).

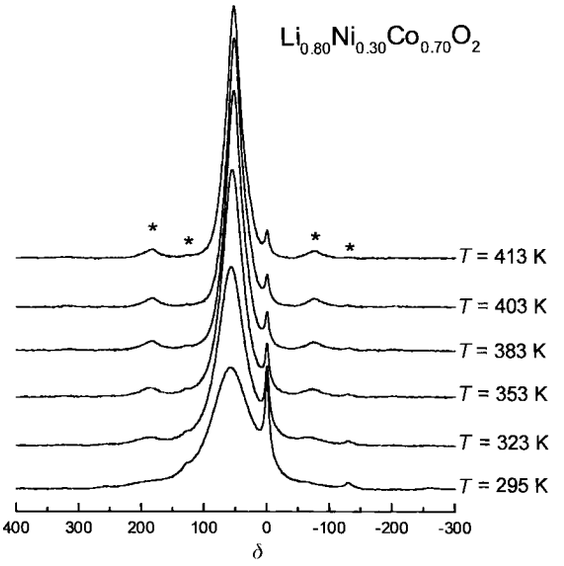

Fig. 8 ^{7}Li MAS NMR spectra of $Li_{0.80}Ni_{0.30}Co_{0.70}O_2$ recorded with the single pulse sequence at various temperatures. Spectra are plotted against an absolute intensity scale, taking into account the number of acquisitions (* denotes spinning side bands).

slightly toward 0 ppm as the magnetic susceptibility decreases. The signal is also sharpened, because mobility increases further with temperature and thus the dipolar interaction is better averaged. The signal at 0 ppm decreases in intensity as the temperature increases, indicating that the timescale of the ionic mobility is becoming close to that of NMR (10^{-6} s). However, even at $T=413$ K, some of this signal remains, indicating that some lithium ions are not yet involved in such mobility at this temperature, the highest we can reach using our MAS NMR set-up.

Further deintercalation. Fig. 5 shows that the shift of the averaged signal, apparent for $x \leqslant 0.80$, decreases toward 0 ppm with lithium deintercalation for $0.70 \leqslant x \leqslant 0.80$ and then increases for $0.40 \leqslant x \leqslant 0.70$. However, the averaged signal is never observed at 0 ppm. If the reduction process associated with lithium deintercalation concerned the Ni^{3+}/Ni^{4+} and Co^{3+}/Co^{4+} redox couples successively, the $Li_{0.70}Ni_{0.30}Co_{0.70}O_2$ phase would be diamagnetic, as all paramagnetic Ni^{3+} ions would be oxidised into diamagnetic Ni^{4+} ions and no diamagnetic Co^{3+} ions would be oxidised yet. However, neither for $x=0.70$ nor for x close to this composition, did we obtain a single non-shifted signal. This fact suggests that the Ni^{3+} and Co^{3+} ion oxidation is competitive in a certain range of composition, so that no diamagnetic phase is formed during lithium deintercalation. This behaviour is also illustrated by the absence of a clear voltage step in the voltage curve at $x=0.70$ (Fig. 3), whereas a more pronounced one is obtained for the $Li_xNi_{0.1}Co_{0.9}O_2$ system, where Co and Ni oxidation are supposed to be successive.[28]

Variable temperature NMR spectra for $Li_{0.70}Ni_{0.30}Co_{0.70}O_2$ and $Li_{0.40}Ni_{0.30}Co_{0.70}O_2$. Fig. 9 shows the evolution of the ^{7}Li MAS NMR signal upon heating of $Li_{0.70}Ni_{0.30}Co_{0.70}O_2$ and $Li_{0.40}Ni_{0.30}Co_{0.70}O_2$, respectively. Upon heating, the averaged signal of the $Li_{0.70}Ni_{0.30}Co_{0.70}O_2$ phase shifts toward higher values. This behaviour is unexpected, since, for paramagnetic compounds, the shift is known to decrease upon heating as the magnetic susceptibility decreases, and for metallic compounds with Pauli susceptibility, the shift is known to be temperature independent. We concluded above that oxidation of Ni^{3+} and Co^{3+} ions is competitive in this composition range. Some paramagnetic Co^{4+} ions thus have to be present in the sample, and we know that localised Co^{4+} ions lead to a very strong directly transferred electron spin density on the Li nucleus, which induces a loss of NMR observation of the lithium ions concerned.[26] The mere presence of some localised Co^{4+} in the sample cannot, therefore, explain the increase of the shift upon heating. The only explanation that we can propose is to consider that heating induces the formation of more and more paramagnetic Ni^{3+} ions. Hopping between cobalt and nickel ions, which can be written as $Ni^{4+}+Co^{3+} \leftrightarrow Ni^{3+}+Co^{4+}$, is thus evidenced and is activated by heating. Such hopping between two transition metal cations has also been evidenced in the $Li(Ni,Fe)O_2$ system.[43,44]

Concerning Fig. 5, we explained the evolution upon deintercalation of the averaged signal toward 0 ppm for $0.70 \leqslant x \leqslant 0.80$ by the decrease of the number of Ni^{3+} ions in the samples, but one may wonder why an increase of the shift is observed for $0.40 \leqslant x \leqslant 0.70$. In Li_xCoO_2, Co oxidation leads to an electronic delocalisation for $x<0.70$ and to a Knight-shifted signal, which shifts further upon deintercalation (in the single-phase domain) similarly to what is observed in Fig. 5 for $x<0.70$.[26] The evolution upon heating of the ^{7}Li MAS NMR signal of the $Li_{0.40}Ni_{0.30}Co_{0.70}O_2$ phase is shown in Fig. 9b. The shift is not strictly temperature independent, as it slightly shifts toward 0 ppm upon heating. Obviously the presence of nickel impedes real long range electronic delocalisation. In order to clarify the origin of the shift for $x \leqslant 0.70$, we studied the electronic properties of the deintercalated materials.

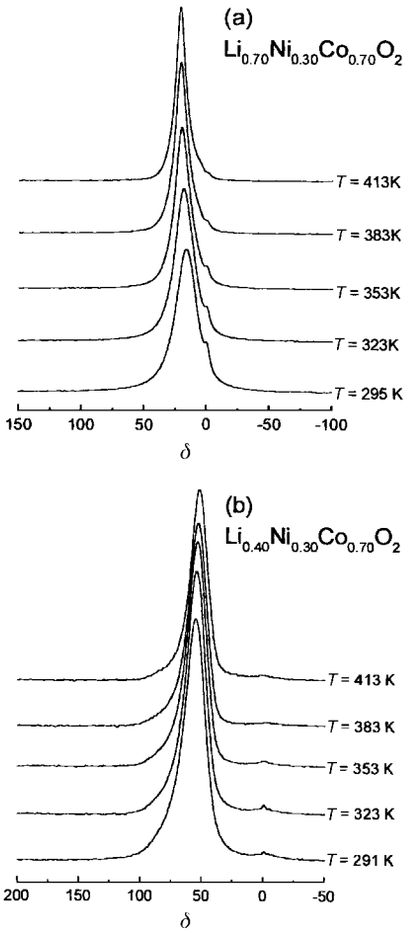

Fig. 9 ^{7}Li MAS NMR spectra of the $Li_{0.70}Ni_{0.30}Co_{0.70}O_2$ (a) and $Li_{0.40}Ni_{0.30}Co_{0.70}O_2$ (b) phases recorded with the single pulse sequence at various temperatures. Spectra are plotted against an absolute intensity scale, taking into account the number of acquisitions.

Electronic properties

Electronic conductivity. Fig. 10 and 11 show the variation of the electronic conductivity *versus* reciprocal temperature for the deintercalated $Li_xNi_{0.30}Co_{0.70}O_2$ phases ($0.71 \leqslant x \leqslant 1$ and $0.40 \leqslant x \leqslant 0.72$). The electronic conductivity is thermally activated for all compositions; it does not strictly obey an Arrhenius law, as the activation energy varies slightly with temperature. The value obtained for $x=1$ is in good agreement with those reported in the literature.[5,45]

For $0.72 \leqslant x \leqslant 1$ the thermal variations of the conductivity are very close to each other, there is only a slight increase in the activation energy (see Table 1) and a slight decrease in the room temperature conductivity upon lithium deintercalation. The values of the activation energy can be compared to those

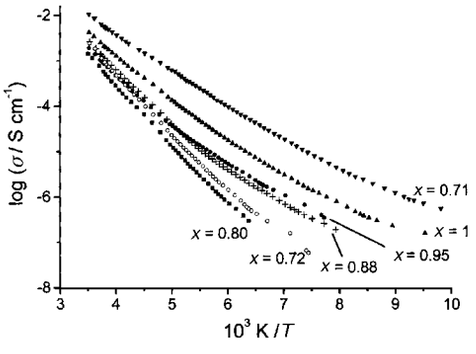

Fig. 10 Variation of the logarithm of the electrical conductivity *vs.* reciprocal temperature of the $Li_xNi_{0.30}Co_{0.70}O_2$ phases ($0.71 \leqslant x \leqslant 1$).

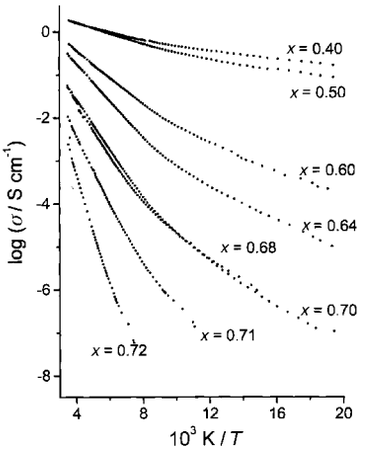

Fig. 11 Variation of the logarithm of the electrical conductivity *vs.* reciprocal temperature of the $Li_xNi_{0.30}Co_{0.70}O_2$ phases ($0.40 \leqslant x \leqslant 0.72$).

obtained with the $Li_xNi_{0.80}Co_{0.20}O_2$ system, where only nickel ions are involved in the redox process.[46]

Conversely, for larger deintercalation amounts ($x < 0.72$), the conductivity increases by several orders of magnitude while the activation energy tends to 0 eV. Clearly, this change in behaviour indicates a change in the oxidation process, suggesting that Co^{3+} ions are oxidised for $x < 0.72$. The conduction electrons are now situated in the Co t_{2g} band, which can overlap through the common edge of the octahedra and lead to delocalisation. In the case of Li_xCoO_2, in agreement with Goodenough's criterion, this leads to a metallic phase for $x < 0.70$.[26] However, the most deintercalated $Li_xNi_{0.30}Co_{0.70}O_2$ phase ($x = 0.40$) is not strictly metallic, since a very small activation energy remains.

Thermoelectronic power. Thermoelectronic power measurements for the various $Li_xNi_{0.30}Co_{0.70}O_2$ compositions were obtained in the temperature range 160–300 K; the results are summarised in Fig. 12. For more clarity, we give in this figure the Seebeck coefficient (α) evolution for some compositions only, which are representative of the general behaviour, and in Fig. 13, the evolution of the Seebeck coefficient at room temperature as a function of lithium deintercalation is shown. The positive Seebeck coefficient obtained for all compositions clearly establishes that electron holes are the prevailing charge carriers. For $x = 1$, the positive sign of the Seebeck coefficient within a Mott–Hubbard band splitting scheme[28,46] seems to indicate that some Ni^{4+} ions are present in the starting material, leading to some electron holes in the Ni^{4+}/Ni^{3+} band.

For the lithium-rich phases, the thermal variations and the absolute values seen for the Seebeck coefficients are characteristic of semiconductors where the number of charge carriers is

Table 1 Electronic conductivity activation energy *vs.* the amount of lithium in $Li_xNi_{0.3}Co_{0.7}O_2$ ($0.40 \leqslant x \leqslant 1$) in the 125–290 K range

$Li_xNi_{0.30}Co_{0.70}O_2$	ΔE/eV
$x = 1$	0.19
$x = 0.95$	0.23
$x = 0.88$	0.24
$x = 0.80$	0.27
$x = 0.72$	0.27
$x = 0.71$	0.15
$x = 0.70$	0.11
$x = 0.68$	0.12
$x = 0.64$	0.08
$x = 0.60$	0.06
$x = 0.50$	0.02
$x = 0.40$	0.02

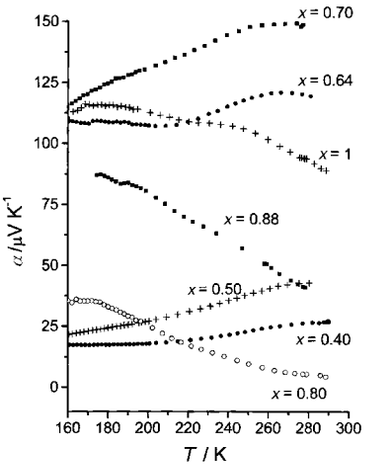

Fig. 12 Thermal variation of the Seebeck coefficient of the $Li_xNi_{0.30}Co_{0.70}O_2$ phases. For more clarity, only the most representative samples are shown here.

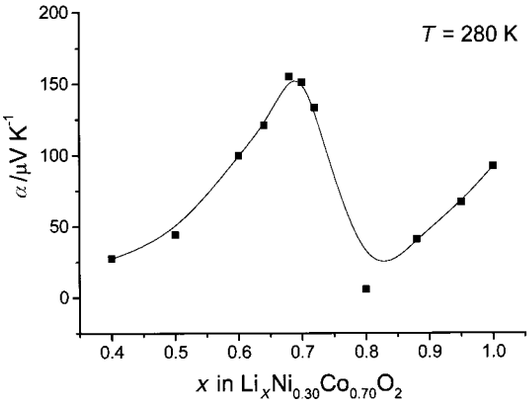

Fig. 13 Room temperature Seebeck coefficient variation *versus* lithium deintercalation for $Li_xNi_{0.30}Co_{0.70}O_2$ phases. The solid line is a guide to the eye.

fixed by the material's composition (except for the $x = 0.80$ material, whose behaviour is not understood). From $x = 1$ to $x = 0.88$ (Fig. 12), the decrease in the Seebeck coefficient shows that the number of charge carriers increases continuously, while the high value of α for $x = 0.70$ shows that there is only a very small amount of charge carriers. Around $x = 0.64$–0.60, the number of charge carriers increases, the electrons remaining localised. In contrast, the low value of the Seebeck coefficient for $x = 0.50$ and $x = 0.40$ and its linear dependence with temperature are characteristic of a tendency to electron delocalisation.

General discussion

If one assumes an ideal energy level diagram, where the Ni^{4+}/Ni^{3+} redox couple does not overlap with the broad Co t_{2g} band, 0.30 electrons per formula unit fill this level. Therefore, for $x = 0.85$, half of the Ni^{3+} ions must be oxidised. The discussion on the electrical properties correlated with the NMR experiments will thus be separated into three $Li_xNi_{0.30}Co_{0.70}O_2$ composition domains.

For $0.85 \leqslant x \leqslant 1$, Ni^{3+} are the only ions oxidised upon lithium deintercalation and the average oxidation state of nickel changes from 3+ to "3.5+" for the two limiting compositions. In this case, electron holes are the expected prevailing charge carriers with an increasing concentration. This is consistent with the evolution of the Seebeck coefficient in this range and with the evolution of the NMR spectra. Indeed NMR shows that Ni^{3+} ions are oxidised and that

mobility increases in the samples. Nevertheless, electrical conductivity measurements show that conductivity decreases and that the activation energy increases with lithium deintercalation in this range. This fact seems to conflict with the increase in mobility in the sample seen by NMR. NMR spectroscopy is sensitive to local mobility, whereas the four probe dc method measures macroscopic electrical conductivity, much influenced by percolation phenomena, due to electronic hopping, and correlation effects, such as those due to the electrostatic repulsion between the polarons. The different behaviour seen by the two methods is, therefore, not so surprising.

For $0.70 \leqslant x \leqslant 0.85$, if Ni^{3+} were the only ions oxidised during lithium deintercalation, the average oxidation state of nickel would change from "3.5+" to 4+ for the two limiting compositions. In this case, the expected prevailing charge carriers are electrons and their number should decrease with lithium deintercalation as the Ni^{3+}/Ni^{4+} rate is smaller than one and more and more Ni^{3+} ions are oxidised. However, our results indicate that the prevailing charge carriers are electron holes and that mobility increases upon lithium deintercalation in this range (activation energy decreases and mobility as seen by NMR increases). Furthermore, the thermal behaviour of the NMR signal for $x = 0.70$ suggests Ni/Co hopping ($Ni^{4+} + Co^{3+} \leftrightarrow Ni^{3+} + Co^{4+}$). Therefore, all the species can be present for this composition, and the question as to which ion is actually oxidised upon deintercalation is not strictly relevant.

For $0.40 \leqslant x \leqslant 0.70$, oxidation of Co^{3+} ions is clearly evidenced by the strong decrease of the activation energy of conductivity upon lithium deintercalation. However, even for $x = 0.40$, the sample is not metallic from the d.c. conductivity point of view, whereas it is close to metallic behaviour for NMR and thermoelectronic measurements.

In Li_xCoO_2 ($0.6 \leqslant x \leqslant 1$), the Co–Co distance was shown to be smaller than the critical distance (R_c) given by Goodenough for electron delocalisation by overlapping of t_{2g} orbitals,[47] leading to metallic compounds for $x \leqslant 0.70$.[26] In $Li_xNi_{0.30}Co_{0.70}O_2$, the Co–Co distance (*i.e.*, the a_{hex} parameters, Fig. 4) is smaller than R_c (for $x = 1$, $d_{Co-Co} = 2.834$ and $R_c = 2.90$ Å and for $x = 0.40$, $d_{Co-Co} = 2.805$ and $R_c = 2.852$ Å). However, the presence of nickel ions obviously hinders long range electronic delocalisation, so that true metallic behaviour is not observed. As concerns NMR, the origin of the shift can thus be assigned to "local" electronic delocalisation between Co ions (Knight shift), but the presence of some Ni^{3+} ion through the Ni/Co hopping discussed above can also add a paramagnetic component to the interaction (and therefore a temperature dependence of the signal for $x = 0.40$ (Fig. 9b)).

Conclusion

Observation of hyperfine interactions makes Li NMR a powerful method for characterising the electronic configuration of the 3d cation in lithium transition element oxides used as positive electrodes for lithium or lithium ion batteries. However, for partially deintercalated materials, mixed valence and Li^+ vacancies allow electronic and ionic hopping which induce exchange phenomena in the NMR signals, making them less straightforward to interpret. The complementary knowledge of the electronic conductivity and thermoelectronic power coefficient leads to a picture of the deintercalation process in $Li_xNi_{0.30}Co_{0.70}O_2$, where the phenomena are not as simple as one might have expected. Indeed, the Ni^{4+}/Ni^{3+} redox couple overlaps with the Co t_{2g} band, all the more as Ni/Co hopping occurs, so that the oxidation of Ni and Co during lithium deintercalation is not so clear-cut. This is probably induced by the presence of isolated Ni in the Co matrix, which cannot take part in the Ni^{4+}/Ni^{3+} hopping, and to the constraints exerted on Co^{3+} ions by their smaller Ni^{4+} neighbours. Furthermore, the presence of Li^+ vacancies with a lower relative mobility tends to pin the oxidised cations in their vicinity. Conversely, for larger deintercalation amounts, the presence of Ni^{4+} ions prevents true long range electronic delocalisation between Co^{3+} and Co^{4+} ions, whereas ^7Li NMR and thermoelectric data give evidence of some extent of delocalisation.

Acknowledgements

The authors wish to thank E. Marquestaut and C. Denage for technical assistance and Région Aquitaine for financial support.

References

1 C. Delmas and I. Saadoune, *Solid State Ionics*, 1992, **53–56**, 370.
2 C. Delmas, I. Saadoune and A. Rougier, *J. Power Sources*, 1993, **43–44**, 595.
3 A. Ueda and T. Ohzuku, *J. Electrochem. Soc.*, 1994, **141**, 2010.
4 R. Alcantara, J. Morales, J. L. Tirado, R. Stoyanova and E. Zhecheva, *J. Electrochem. Soc.*, 1995, **142**, 3997.
5 I. Saadoune and C. Delmas, *J. Mater. Chem.*, 1996, **6**, 193.
6 D. Caurant, N. Baffier, B. Garcia and J. P. Pereira-Ramos, *Solid State Ionics*, 1996, **91**, 45.
7 W. Li and C. Currie, *J. Electrochem. Soc.*, 1997, **144**, 2773.
8 R. Alcantara, P. Lavela, J. L. Tirado, R. Stoyanova and E. Zhecheva, *J. Electrochem. Soc.*, 1998, **145**, 730.
9 J. Cho, G. Kim and H. S. Lim, *J. Electrochem. Soc.*, 1999, **146**, 3571.
10 E. Zhecheva and R. Stoyanova, *Solid State Ionics*, 1993, **66**, 143.
11 A. Rougier, C. Delmas and A. V. Chadwick, *Solid State Commun.*, 1995, **94**, 123.
12 T. Nakagome and I. Nakaï, *Denki Kagaku*, 1998, **66**, 727.
13 M. Ménétrier, A. Rougier and C. Delmas, *Solid State Commun.*, 1994, **90**, 439.
14 K. R. Morgan, S. Collier, G. Burns and K. Ooi, *J. Chem. Soc., Chem. Commun.*, 1994, 1719.
15 C. Marichal, J. Hirschinger, P. Granger, M. Ménétrier, A. Rougier and C. Delmas, *Inorg. Chem.*, 1995, **34**, 1773.
16 P. Mustarelli, V. Massarotti, M. Bini and D. Capsoni, *Phys. Rev. B*, 1997, **55**, 12018.
17 B. Gee, C. R. Horne, E. J. Cairns and J. A. Reimer, *J. Phys. Chem. B*, 1998, **102**, 10142.
18 Y. J. Lee, F. Wang and C. P. Grey, *J. Am. Chem. Soc.*, 1998, **120**, 12601.
19 N. Treuil, C. Labrugere, M. Menetrier, J. Portier, G. Campet, A. Deshayes, J. C. Frison, S. J. Hwang, S. W. Song and J. H. Choy, *J. Phys. Chem. B*, 1999, **103**, 2100.
20 B. Ouyang, X. Cao, H. W. Lin, S. Slane, S. Kostov, M. d. Boer and S. G. Greenbaum, *Mater. Res. Soc. Symp. Proc.*, 1995, **369**, 59.
21 M. Carewska, S. Scaccia, S. Arumugam, Y. Wang and S. Greenbaum, *Solid State Ionics*, 1997, **93**, 227.
22 T. J. Boyle, D. Ingersoll, T. M. Alam, C. J. Tafoya, M. A. Rodriguez, K. Vanheudsen and D. H. Doughty, *Chem. Mater.*, 1998, **10**, 2270.
23 R. Alcantara, P. Lavela, J. L. Tirado, E. Zhecheva and R. Stoyanova, *J. Electroanal. Chem.*, 1998, **454**, 173.
24 M. P. J. Peeters, M. J. Van Bommel, P. M. C. Neilen-ten Wolde, H. A. M. Van Hal, W. C. Keur and A. P. M. Kentgens, *Solid State Ionics*, 1998, **112**, 41.
25 N. Imanishi, M. Fujiyoshi, Y. Takeda, O. Yamamoto and M. Tabuchi, *Solid State Ionics*, 1999, **118**, 121.
26 M. Ménétrier, I. Saadoune, S. Levasseur and C. Delmas, *J. Mater. Chem.*, 1999, **9**, 1135.
27 S. Levasseur, M. Menetrier, E. Suard and C. Delmas, *Solid State Ionics*, 2000, **128**, 11.
28 I. Saadoune, M. Ménétrier and C. Delmas, *J. Mater. Chem.*, 1997, **7**, 2505.
29 Y. J. Lee, F. Wang, S. Mukerjee, J. McBreen and C. P. Grey, *J. Electrochem. Soc.*, 2000, **147**, 803.
30 P. Dordor, E. Marquestaut and G. Villeneuve, *Rev. Phys. Appl.*, 1980, **15**, 1607.
31 H. M. McConnell and R. E. Roberston, *J. Chem. Phys.*, 1958, **29**, 1361.
32 H. M. McConnell and D. B. Chesnut, *J. Chem. Phys.*, 1958, **28**, 107.
33 I. Bertini and C. Luchinat, *NMR of Paramagnetic Molecules in*

Biological Systems, The Benjamin/Cummings Publishing Company Inc., Menlo Park, CA, 1986.
34 G. Engelhardt, M. Feuerstein, P. Sieger, D. Markgraber, G. Stucky and V. Srdanov, *Chem. Commun.*, 1996, 729.
35 J. B. Goodenough, *Magnetism and the Chemical Bond*, John Wiley & Sons, New York and London, 1963.
36 G. Maruta, S. Takeda, R. Imachi, T. Ishida, T. Nogami and K. Yamaguchi, *J. Am. Chem. Soc.*, 1999, **121**, 424.
37 H. Heise, F. H. Köhler, F. Mota, J. J. Novoa and J. Veciana, *J. Am. Chem. Soc.*, 1999, **121**, 9659.
38 R. Stoyanova, E. Zhecheva, E. Kuzmanova, R. Alcantara, P. Lavela and J. L. Tirado, *Solid State Ionics*, 2000, **128**, 1.
39 J. N. Reimers and J. R. Dahn, *J. Electrochem. Soc.*, 1992, **139**, 2091.
40 W. Li, J. N. Reimers and J. R. Dahn, *Solid State Ionics*, 1993, **67**, 123.
41 A. Maazaz, C. Delmas and P. Hagenmuller, *J. Inclusion Phenom.*, 1983, **1**, 45.
42 C. P. Slichter, *Principles of Magnetic Resonance*, 3rd edn., Springer-Verlag, Berlin, 1992.
43 G. Prado, A. Rougier, L. Fournès and C. Delmas, *J. Electrochem. Soc.*, 2000, **147**, 2880.
44 G. Prado, E. Suard, L. Fournès and C. Delmas, *J. Mater. Chem.*, 2000, **10**, 2553.
45 J. Molenda, P. Wilk and J. Marzec, *Solid State Ionics*, 1999, **119**, 19.
46 I. Saadoune and C. Delmas, *J. Solid State Chem.*, 1998, **136**, 8.
47 J. B. Goodenough, *Prog. Solid State Chem.*, 1971, **5**, 278.